EMA-90-R-51

EMA ELECTRO MAGNETIC APPLICATIONS, INC.
P.O. Box 260263
Denver, CO 80226-2091
(303) 980-0070

MICROSTRUCTURAL MODELING OF ELECTRICAL BREAKDOWN IN SOLID FUEL PROPELLANTS

Prepared by:

Ronal W. Larson
Paul D. Beale
John D. Curry
Fred Eriksen
Michael Frisoni
Mark F. Gyure

Submitted to:

Army Research Office
U.S. Army Laboratory Command
P.O. Box 12211
Research Triangle Park, NC 27708-2211

Final Report for ARO Project #P-24927-EG-S
Contract No. DAAL03-87-C-0021

March 23, 1993

MASTER COPY KEEP THIS COPY FOR REPRODUCTION PURPOSES

REPORT DOCUMENTATION PAGE

Form Approved
OMB No 0704-0188

1. AGENCY USE ONLY (Leave blank)	2 REPORT DATE	3 REPORT TYPE AND DATES COVERED
	March 23, 1993	Final 14 Aug 87-14 Oct 90

4. TITLE AND SUBTITLE

Microstructural Modeling of Electrical Breakdown in Solid Fuel Propellants

5. FUNDING NUMBERS

DAAL03-87-C-0021

6. AUTHOR(S)

Ronal W. Larson
Paul D. Beale
John D. Currey
Fred Eriksen
Michael Frisoni
Mark E. Gyure

7. PERFORMING ORGANIZATION NAME(S) AND ADDRESS(ES)

EMA
P.O. Box 260263
Denver, CO 80226-2091

8 PERFORMING ORGANIZATION REPORT NUMBER

9. SPONSORING/MONITORING AGENCY NAME(S) AND ADDRESS(ES)

U. S. Army Research Office
P. O. Box 12211
Research Triangle Park, NC 27709-2211

10 SPONSORING/MONITORING AGENCY REPORT NUMBER

ARO 24927.4-EG-S

11. SUPPLEMENTARY NOTES

The view, opinions and/or findings contained in this report are those of the author(s) and should not be construed as an official Department of the Army position, policy, or decision, unless so designated by other documentation.

12a DISTRIBUTION/AVAILABILITY STATEMENT

Approved for public release; distribution unlimited.

12b DISTRIBUTION CODE

13 ABSTRACT *(Maximum 200 words)*

The subject matter in this report is an analytical treatment of microstructural aspects of Electrostatic Discharge (ESD) ignition of solid rocket motors. ESD hazards of the type described herein are now well known to the solid propellant industry. Since 1985, two accidents involving solid rocket motors have caused the loss of eight lives. These are now accepted to have been initiated by ESD, causing ESD to have become the leading safety hazard within the solid propellant industry;

The report describes features of solid propellants that make them particularly susceptible to ESD. Primary emphasis has been placed on microstructural modeling to better understand how to mitigate these hazards by understanding the details of the hazard.

(Continued on reverse side)

14 SUBJECT TERMS	15 NUMBER OF PAGES
Propellants, Solid Fuel Propellants, Electrostatic Discharge Ignition, Ignition, Solid Rocket Motors, Safety Hazards, Solid Propellants	16 PRICE CODE

17 SECURITY CLASSIFICATION OF REPORT	18 SECURITY CLASSIFICATION OF THIS PAGE	19 SECURITY CLASSIFICATION OF ABSTRACT	20 LIMITATION OF ABSTRACT
UNCLASSIFIED	UNCLASSIFIED	UNCLASSIFIED	UL

Attempts have been made in this and a companion doctoral thesis to explain (among other things) effects of time (or frequency), propellant formulation, temperature, pressure, and relative humidity. This report explains, but is not intended as a final definitive explanation of, much of the experimental phenomena that is summarized herein.

EMA-90-R-51

EMA ELECTRO MAGNETIC APPLICATIONS, INC.
P.O. Box 260263
Denver, CO 80226-2091
(303) 980-0070

MICROSTRUCTURAL MODELING OF ELECTRICAL BREAKDOWN IN SOLID FUEL PROPELLANTS

Prepared by:

Ronal W. Larson
Paul D. Beale
John D. Curry
Fred Eriksen
Michael Frisoni
Mark F. Gyure

Submitted to:

Army Research Office
U.S. Army Laboratory Command
P.O. Box 12211
Research Triangle Park, NC 27708-2211

Final Report for ARO Project #P-24927-EG-S
Contract No. DAAL03-87-C-0021

March 23, 1993

TABLE OF CONTENTS

LIST OF FIGURES

LIST OF TABLES

PREFACE

This final report is a summary of the final portion of the work performed on this contract which deals with modeling the ESD-caused ignition of solid propellants. A summary of the prior work was already submitted in an interim report that preceded an ARO-sponsored workshop, held in Nashville, Tennessee on April 17 and 18, 1989, devoted primarily to the question of ignition following an ESD breakdown event. That interim report dealt only peripherally with ignition.

However, there was always an intent to consider ignition in the final year of the contract, so this document adds material on that subject as well as containing several new items of research not reported in a thesis, that is the other main output of this contract.

The authors wish to thank ARO's Project monitor, Dr David Mann, for taking a strong interest in the subject matter of this project.

CHAPTER 1
EXECUTIVE SUMMARY

This document is the final report for a three year study performed at Electromagnetic Applications, Inc (EMA) for the U.S. Army Research Office (ARO). The subject matter is an analytical treatment of microstructural aspects of Electrostatic Discharge (ESD) ignition of solid rocket motors. This report, and a companion document (Dr. Mark Gyure's thesis) [1], are an expansion of an interim report covering similar material, released in mid 1989 [2].

ESD hazards of the type described herein are now well known to the solid propellant industry [2], although this was less so at the time of our original proposal to ARO in 1986. Since 1985, two accidents involving solid rocket motors have caused the loss of eight lives. These are now accepted to have been initiated by ESD, causing ESD to have become the leading safety hazard within the solid propellant industry;

This report describes features of solid propellants that make them particularly susceptible to ESD Primary emphasis has been placed on microstructural modeling to better understand how to mitigate these hazards by understanding the details of the hazard.

Attempts have been made in this and the companion doctoral thesis [1] to explain (among other things) effects of time (or frequency), propellant formulation, temperature, pressure, and relative humidity This report explains, but is not intended as a final definitive explanation of, much of the experimental phenomena that is summarized herein. In summary, we can make the following general statements that are supported by the (primarily) microscopic analyses within this ARO contract.

1. As work has been performed on the electrostatic breakdown and ignition of solid propellants in response to the two accidents, it has become clear that there are good macroscopic and microscopic reasons for ESD to be a serious hazard for solid propellants. Based on both static and transient macroscopic simulations by EMA (not the subject of this report), the propellant fields from realistic charge densities can sometimes exceed those known to cause breakdown in small experimental samples. From a modeling standpoint, the analysis of the field distribution is not simple, but good accuracy is possible, and there are few doubts that hazardous situations can occur

2. From the microscopic viewpoint, the general features are also understood Microscopic modeling is able to explain, primarily through the statistical details of the proximity of the aluminum particles, many of the experimental breakdown variations. However, the details of the behavior of propellant

breakdown fields, conductivity and permittivity as a function of time (or frequency) and temperature are only incompletely understood.

3. Among the various macromodeling techniques, the finite element technique has shown the most significant advantages in terms of accuracy, ease of interaction during problem set-up, ease of obtaining solution, quality of display and interpretation of results, short computing time, and total solution time. However, the finite element method has not been of significant value in studying random media (except as it occasionally is used as in the above ways), since it is not usually used for multiple runs with varying parameters(such as in sequential breakdown discussed in [Ref 1] For this study of random media, resort is largely made to boundary element methods [1].

Among the other conclusions, mostly discussed in detail in [Ref. 1]:

Breakdown fields (at least in the cases studied to date) are linearly related to average interparticle spacings in both highly structured and random media. The relationship is simpler than originally expected.

Formulas have been obtained for interparticle fields between spheres with acceptable accuracy and speed of solution.

New insights have been gained on the effect of differential conductivity in explaining both field enhancement and resistivity vs. time experiments.

Much of the material that would normally appeared in this final report have already appeared in Reference [2], and virtually none will therefore be repeated here. A brief overview was given in Section 2 of [2] of the four major parts of the breakdown phenomenon. This was followed in its Section 3 by a description of a number of modeling techniques and results that are primarily useful in macroscopic modeling, but with emphasis on their use in microscopic modeling. Sections 4 and 5 dealt with major portions of Dr Gyure's thesis, which now appear as a separate component of this final report [1] Brief comments were made in Section 6 of a number of topics of importance to understanding the physical aspects of breakdown not covered in the thesis; this work was performed by other investigators working on the project. The final section of the interim report [2] gave some of the team's views on items that were covered in the ARO-sponsored workshop [3] for which the interim report was prepared That section has been retained and expanded as part of this document.

A major portion of the team effort was the support of Mr (now Dr.) Mark Gyure in obtaining his doctoral degree (in Physics) at the University of Colorado That work was under the direction of Dr. Paul Beale, who has also authored some sections in the present volume. Mark Gyure's doctoral work, in its entirety, is contained in the

separate report [1]. He has also contributed a short section on energy considerations related to his thesis work in this final report.

CHAPTER 2

PARTICLE SEPARATIONS AND EXPERIMENTAL VERIFICATION

(Prepared by Dr. Paul Beale)

One of the primary results[4-6] of the electrostatic breakdown modeling is the simple connection between the dielectric breakdown strength of a metal-loaded dielectric and the average nearest-neighbor surface-to-surface distance between the metallic particles in the composite.

$$E_b = E_b^{binder} \frac{d}{d + D} \tag{2.1}$$

The breakdown field, E_b, is directly proportional to the breakdown field of the binder. The proportionality constant depends on, d, the average nearest neighbor distance between metal particles and, D, the diameter of the metal particles. Unfortunately, the distance between particles in a random composite is difficult to measure. Instead we determined this value by appealing to known mathematical properties of the correlations between hard spherical particles in the statistical mechanics of simple fluids.

Let $\rho = N/V$ be the number density of particles in a volume V. The pair correlation function g(r) is defined by $4 \pi r^2 \rho\, g(r)\, dr$; it is the probability that the center of a particle is located at a distance between r and r+dr from the center of a chosen particle. The average nearest neighbor distance can be determined from the distribution function for particle separations. Let p(r) dr be the probability that the closest neighbor of a given particle is at a distance between r and r+dr from a given particle. It is not too difficult to show that

$$p(r) = 4\pi\rho\, r^2\, g(r) \exp\left[4\pi\rho \int_0^{\infty} g(r')\, r^2\, dr \right]. \tag{2.2}$$

From this distribution function, the determination of d is easy.

$$d = \int_0^{\infty} r\, p(r)\, dr \; - \; D \tag{2.3}$$

Now, the goal of the microstructural theory is to determine the pair correlation function g(r) The added difficulty is the situation we have with propellants is that the composite is composed of different types and sizes of particles. Let N_i be the number of particles of type i with diameter D_i. The number densities of the different components are given by $\rho_i = N_i/V$. There will be several different pair correlation functions corresponding to the correlations between particles of type i and particles of type j. Let $\rho_i\, \rho_j\, g_{ij}(r_1 - r_2)\, d^3r_1\, d^3r_2$ be the probability that a

particle if type i is located inside volume element d^3r_1 located at position r_1 and a particle of type j is located inside volume element d^3r_2 located at position r_2. The nearest neighbor probability distribution functions are $p_{ij}(r)\,dr$ is the probability that a particle of type i has its nearest neighbor of type j at a distance between r and r+dr. This is gotten from the pair correlation functions $g_{ij}(r)$ by the relation

$$p_{ij}(r) = 4\pi\rho_j\, g_{ij}(r) \exp\left[4\pi\rho_j \int_0^\infty g_{ij}(r')^2\, dr \right] \tag{2.4}$$

The goal of our microstructural theory is to determine the pair correlation functions and from those to determine the nearest neighbor spacing between metal particles. The model that will be assumed is that the particles are hard spheres of diameter D_i with number densities n_i.

The calculation of the pair correlation functions proceeds with the Boltzmann assumption that any configuration of particles which is possible (no hard spheres overlap) has equal *a priori* probability. Since this is also the basis of all of statistical mechanics, we will make use of the statistical mechanics of simple liquids to determine the pair correlation functions.[7] The particular approach used is based on the properties of the direct correlation functions $c_{ij}(r)$ which are defined by the Ornstein-Zernike equation.[8]

$$g_{ij}(r) - 1 = c_{ij}(r) + \sum_k \rho_k \int c_{ik}(r')\,[\, g_{kj}(r-r') - 1\,]\, dr \tag{2.5}$$

This in itself contains no new information. The calculation of the pair correlation functions depends on being able to close these equations with a means of specifying another constraint on the direct correlation functions. The constraint we use is the Perkus-Yevick equation[7-11] which for hard spheres states that the direct correlation function $c_{ij}(r)$ is zero for all $r > (D_i + D_j)/2$. This constraint allows the exact calculation of all of the direct correlation functions and pair correlation functions for up to two different sphere sizes. This approximation is well-tested in the statistical mechanics of simple liquids and is known to be quite accurate even at very high particle densities near the phase transition to a solid crystalline phase.[7]

Lebowitz gives an exact expression for the direct correlation functions.[11] They are of the form

$$-c_{11}(r) = \begin{cases} a_1 + b_1 r + d r^3 & r < D_1 \\ 0 & r > D_1 \end{cases} \tag{2.6a}$$

$$c_{22}(r) = \begin{cases} a_2 + b_2 r + d r^3 & r < D_2 \\ 0 & r > D_2 \end{cases} \qquad (2.6b)$$

$$c_{12}(r) = \begin{cases} a_1 & r<1 \\ a_1 + \dfrac{b x^2 + 4 1 d x^3 + d x^4}{r} & 1<r<D_{12} \\ 0 & r > D_{12} \end{cases} \qquad (2.6c)$$

where x=r-1 and the coefficients a_i , b_i, b and d are given in Lebowitz's paper [11]

The Fourier transforms of the direct correlation functions are defined by

$$C_{ij}(k) = \frac{4\pi}{k} \int_0^\infty r\, c_{ij}(r)\, \sin(kr)\, dr \qquad (2.7)$$

and the Fourier transforms of the pair correlation function are defined by

$$h_{ij}(k) = \frac{4\pi}{k} \int_0^\infty r\, [g_{ij}(r) - 1]\, dr \qquad (2.8)$$

In Fourier transform space the Ornstein Zernike equation has the form

$$h_{ij}(k) = C_{ij}(k) + \sum_1 \rho_n\, C_{in}(k)\, h_{nj}(k) \qquad (2.9)$$

This equation can be solved for the Fourier transforms of the pair correlation functions $h_{ij}(k)$ Finally the determination of the pair correlation functions is accomplished by inverse Fourier transforming

$$g_{ij}(r) = 1 + \frac{1}{2\pi^2 r} \int_0^\infty k\, h_{ij}(k)\, \sin(kr)\, dk \qquad (2.10)$$

Note that this step cannot be done analytically (at least not easily) so this final step must be done numerically using a fast Fourier transform routine. Once this is accomplished equations (3) and (4) can be evaluated numerically to determine the nearest neighbor spacings in the composite

Our theoretical claim in equation (1) that the breakdown field scales simply with the nearest-neighbor spacing can be tested with experimental data. Table 2.1 shows the mixture proportions and breakdown field for a series of inert propellants mixed by Gibson at Edwards AFB and tested by Covino and Hudson at China Lake NWC.[12] In the samples, the ammonium perchlorate was replaced by NaCl. From the mixture proportions the pair correlation functions and nearest-neighbor spacings were determined using the above procedure. The NaCl particles were assumed to be 100 times larger than the Al particles. Figures 2.1 - 2.3 shows the pair correlation functions for sample KJ-15 and Figure 2.4 shows the Al-Al nearest neighbor distribution function. The calculated nearest neighbor spacing for this sample was 0.045 D_1. Figure 2.5 shows the experimental breakdown field plotted vs $d/(D_{Al} + d)$. Equation (2.1) predicts that the data should fall on a straight line with slope E_b^{binder} and intersect the origin. As is evident, the data is well approximated by a straight line (which intersects the origin as predicted) and that the slope of 19MV/m is in good agreement with the subsequently determined experimental binder breakdown field of 23MV/m. This excellent agreement between theory and experiment is very encouraging and constitutes a quantitative theoretical approach for determining the dielectric breakdown strength of random metal-loaded dielectric composites.

Table 2.1

Mixture Proportions and Breakdown Fields for Inert Propellants

Sample	Volume % 3 micron Al	Volume % NaCl	Breakdown Field (MV/m)	d/D
KJ-17	3.0	55.7	4.7	0.327
KJ-14	12.7	47.5	1.65	0.087
KJ-15	22.4	35.9	0.75	0.045
KJ-16	33.4	25.0	0.45	0.025
KJ-18	54.7	0.0	0.25	0.0126

The experimental breakdown field plotted versus the theoretically determined average nearest neighbor distance. The data is shown in Table 2.1. The slope of the line is 18 MV/m which is the theoretical prediction of the breakdown field of the binder. The subsequently determined breakdown field for the binder was 23 MV/m.

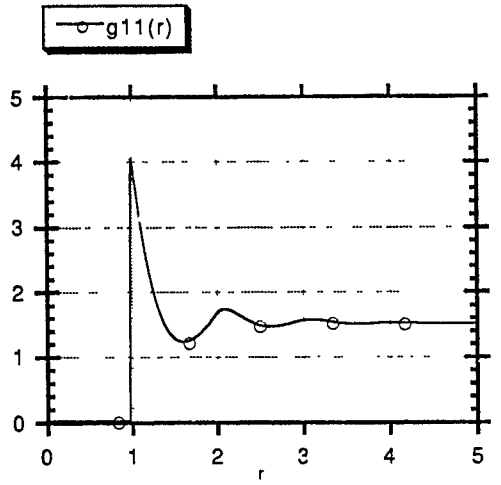

Figure 2.1 The Aluminum-Aluminum Pair Correlation Function for KJ-15

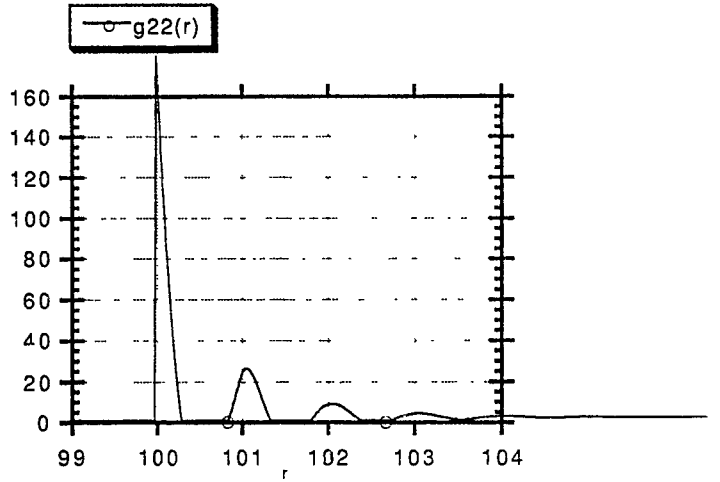

Figure 2.2 The NaCl-NaCl Pair Correlation Function for KJ-15

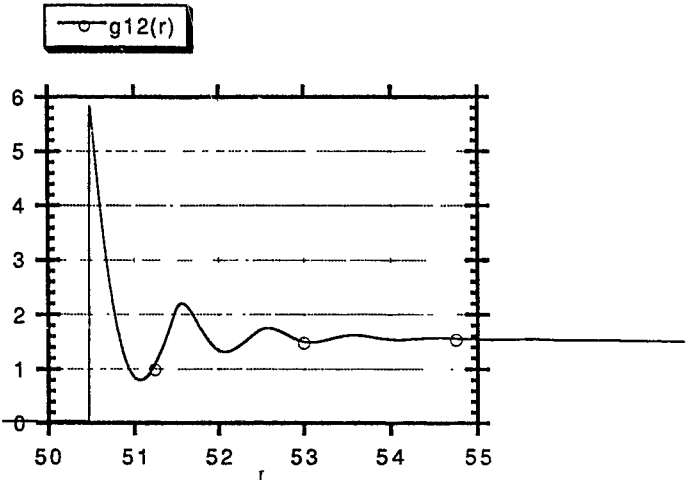

Figure 2.3 The Aluminum-NaCl Pair Correlation Function for KJ-15

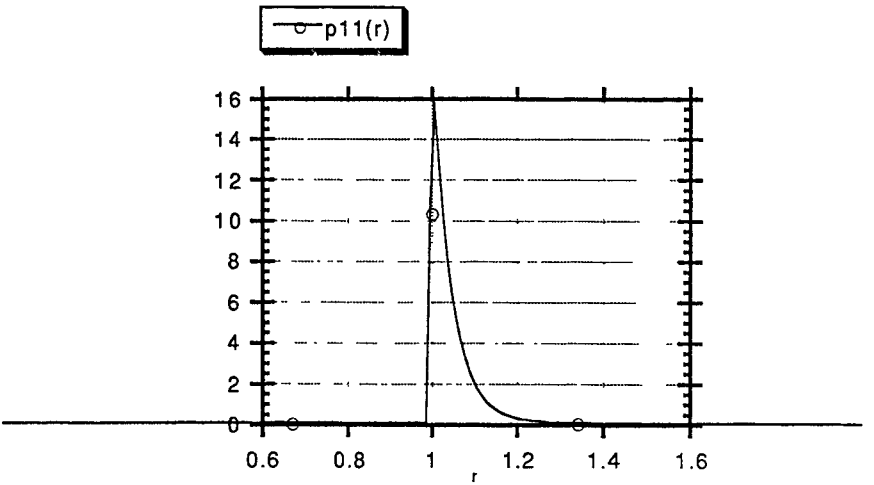

Figure 2.4 The Aluminum-Aluminum Nearest Neighbor Distance Distribution Function for KJ-15

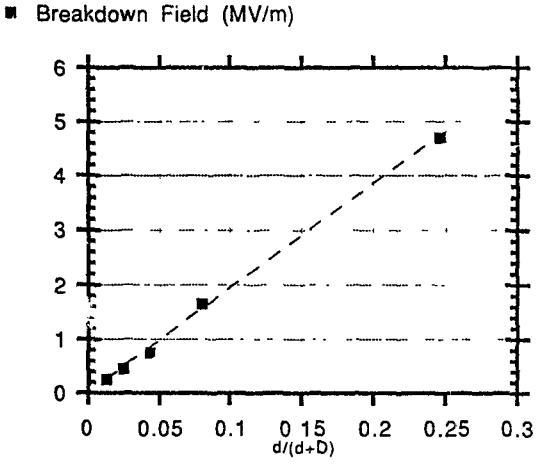

Figure 2.5 Test of Theory on China Lake Data

CHAPTER 3

ENERGY FOUND IN MICROSCOPIC MODELING

(Prepared by Dr. Mark Gyure, as an Extension of Work in his Thesis [1])

The work of Reference [1] is primarily addressing the problem of breakdown in randomly inhomogeneous materials and not the problem of ignition of actual materials such as solid rocket propellants. The breakdown simulations described in this work do provide enough data, however, to estimate the energy released in local breakdown events and this information should be useful, if not essential, to anyone interested in modeling ignition processes in these materials.

The ignition problem of interest to the aerospace community can be stated in the following way If a solid rocket propellant experiences dielectric breakdown, what is the probability that the propellant will also ignite and burn? Or put another way, is electrical breakdown a sufficient condition for ignition of a given propellant or can breakdown occur without ignition? The problem of ignition of solid rocket propellants due to dielectric breakdown is a very difficult one for several reasons that will not be discussed in detail here. Briefly, the problems encountered are the inhomogeneity of the material and the difficulty of modeling a system of sufficient size The ignition question is primarily a thermodynamic one; the likely scenario for ignition based on a dielectric breakdown event is as follows In each local breakdown, some amount of energy is dissipated into the propellant through Joule heating as charge is transferred between the aluminum particles and some energy is also dissipated through radiation from the discharge arc itself. In order for ignition to occur, this energy must be deposited in such a way as to raise the temperature of the material surrounding the arc to a high enough value for a long enough time for a self sustaining chemical reaction to occur in the propellant. How high this temperature must be and how long it must be maintained is a function of the thermodynamic/chemical properties of the materials involved and the geometry of the propellant at the microstructural level. These are issues that will not be addressed here, but one key parameter that is needed to begin any analysis of the ignition question is an estimate of how much energy is dissipated in a local breakdown or sequence of local breakdowns. Such an estimate can be made from the breakdown simulations described in Reference [1] and will be the subject of this section

At each step in the sequence of local breakdowns, two important quantities are known that have direct relevance to the amount of energy released during such an event. First, the voltage difference between the metallic particles is known just before the breakdown event from the electrostatic solution for the potentials In addition, the net charge on the particles is known both before and after the local breakdown when the new electrostatic solution is found. If the particles were not part of any breakdown path before the local breakdown in question, then the net charge before the breakdown was, of course, zero From these parameters, the energy can be estimated straightforwardly by taking the net charge transferred across the gap between the particles and multiplying that charge

by the voltage drop that existed across that gap before the breakdown This is only an estimate, of course, the exact value for the energy released is a function of the exact particle geometry and local fields This is an order of magnitude estimate only, but one which may be useful as a starting point for more complicated and detailed ignition modeling.

The energy released in each local breakdown for the 3D simulations of 135 spheres was estimated from the simulation data as described above The main conclusion is that the energy released during a local breakdown between particles is on the order of 10 to 100 picojoules This estimate comes from assuming that the particles have a radius of ten microns and that the electric field between the particles just before breakdown is right at the breakdown field of the binder which is taken to be 20 MV/m. The simulation data can be scaled to give values for the energy based on any particle size and any field between the particles. If the particles are larger that 20 microns in diameter, then the energy released is larger because the charge transfer is larger Also if the field between the particles is larger than the breakdown field of the binder, this also increases the energy released. The basic relationship which scales the energy is

$$U = C E^2 a^3$$

where U is the energy, E is the field between the particles (or the applied field), a is the particle radius which also determines the system size for a given volume fraction and number of particles, and C is a constant of proportionality Hence for any field or particle size, the energy can be estimated from the simulation data.

Another conclusion suggested by the simulation data is that more energy is released in those breakdowns that occur later in the breakdown process than the initial breakdowns. Again this assumes that the field between the particles undergoing breakdown is held at a fixed value of 20 MV/m regardless of when they break down This result occurs because more energy is available in a region where the field between two particles is fixed and the distance between them is increased. Recall that the distance between particles that undergo breakdown generally increases as the breakdown process continues. With the assumption of a 20 MV/m field between particles and 20 micron diameter particles, the energy released during breakdown in samples at the lowest volume fractions of 20% ranges from 5 pJ in the early breakdowns to more than 50 pJ for breakdowns occurring at later stages in the breakdown process

For volume fractions of 50%, the highest studied for 3D systems, the energy released ranges from around 5 pJ for initial breakdowns to only 10 pJ later in the breakdown sequence This is again easily interpreted: at higher volume fractions, the average particle separation distance decreases so that the distances involved in breakdowns later in the sequence are still quite small whereas the distances between particles in the initial breakdowns are quite small in either case A final comment is that the energy stored between two spheres placed in a known, uniform field can be calculated exactly after finding the capacitance between the spheres In the case of a 20 MV/m field, the energies

are on the order of tens of picojoules for separation distances like those encountered in the breakdown simulations. This is not unexpected since the energy stored in this two sphere system should be the same order of magnitude as the energy stored between two spheres in a random configuration.

In summary, the modeling of ignition processes in solid rocket propellants is a complicated problem involving the conversion of stored electrical energy to heat and the subsequent thermodynamic transfer of this heat to the material which may or may not cause ignition. Any ignition modeling therefore depends on knowing the magnitude of energy released in a breakdown process. This energy is on the order of 10 to 100 picojoules for local breakdowns between particles of 20 microns in diameter, depending on the distance between the particles which is larger at small volume fractions and smaller at large volume fractions. Hence, although propellants with a higher volume fraction of aluminum break down easier, more energy is released in the breakdown of propellants with a lower volume fraction of aluminum. Whether this amount of energy is large enough and can be deposited rapidly enough to cause an ignition process to begin is a question in need of further investigation. In part it is covered in Chapter 4.

CHAPTER 4
IGNITION OF SOLID PROPELLANTS

4.1 Introduction

Analyses of ESD-caused ignition (as opposed to breakdown) of solid propellants must include an investigation of:

1. Electrical energy available to start ignition in typical system-level geometries,
2. Electrical energy deposition in typical arcs as a function of sample size and characteristics such as resistance,
3. Electrical energy, power, and time requirements for arcs to cause ignition,
4. Resistive loss mechanisms in arcs, and,
5. Physical properties of solid propellants (e.g., heat capacity) that relate to ignition

The above considerations can be broken up into two levels of investigation a system or macroscopic level, and a local or microscopic level. In earlier sections, we discussed the electrostatics of system level ESD charging Our discussion of the local or microscopic level is contained in Sections 4.2 and 4.3, and will be broken up into the arc electrodynamics and the ignition physics. Section 4.2 addresses the relationship between energy and properties of the arc, and Section 4.3 discusses the basic laws relating to propellant ignition, and the extrapolation of current ignition threshold data to the short time scale of micro discharges.

We note that the ESD community often uses the words vulnerability and susceptibility to describe aspects of the breakdown and ignition problem. In our terminology, the available energy on a system level is related to vulnerability, and the energy in the micro discharge (between particles in metal loaded propellants, for example) is related to susceptibility.

A primary objective of this chapter is to provide a set of nomograms to quantify the relationships between the various important ignition parameters. There are many parameters to keep in mind, including power, power density, energy, energy density, voltage, charge, current, resistance, capacitance, time, and charge density, for example. There is generally a physical property of an object that is a parameter for curves on the nomogram Examples of such parameters are arc length, capacitance, spark gap distance, source charge density, and resistance It is hoped that these nomograms will help the reader to appreciate quantitatively the many relationships that exist at the system and local levels. Additional information that may be helpful in understanding the concepts in this paper are contained in Reference [2, 13, 14]

4.2 System Level Electromagnetic Principles

At the system level we will show the relation between the internal voltages and fields, and the external sources which are charge densities. The physical properties of the system that relate these quantities are capacitance and system level gap dimension. The mathematical relations between the variables are:

$$Q = Q_S A \tag{4.1a}$$

$$V = Q/C \tag{4.1b}$$

$$V = Ed \tag{4.1c}$$

$$U_a = 1/2\ C\ V^2 \quad (\text{or } 1/2\ Q\ V) \tag{4.1d}$$

where

- Q = total charge (coulombs)
- Q_S = charge density per area (coulombs per square meter)
- A = area (square meters)
- V = voltage across the system (volts)
- C = capacitance of the system holding the source charges (farads)
- E = magnitude of electric field (volts /m)
- d = system level gap (distance over which E is developed) (meters), and
- U_a = available energy (joules)

Figure 4.1 shows these equations in graphical form (nomograms), using log-log scales for each nomogram For example, Figure 4.1a (the right-hand figure) shows Eq 4.1a, where we can enter a known area A (abscissa) and an assumed charge density Q_S, to obtain a specified charge. These nomograms allow one to more clearly visualize the relationship of the many system level electromagnetic parameters.

In the example, we assume an area of two square meters and a charge density of Q_S=15 μcoulombs per square meter. This gives a total charge Q of 30 μcoulombs. Traveling left from Figure 4.1a to Figure 4.1b gives a voltage if the total equivalent capacitance is known. In our example case, an assumed value of 1 nanofarad would lead to a voltage of 30 kilovolts With this voltage, average fields (Figure 4.1c) and energies (Figure 4.1d) can also be established. In the example, a field of 1 MV with a gap of 3 cm as shown in Figure 4.1c gives an energy of 0 45 joules with 1 nF

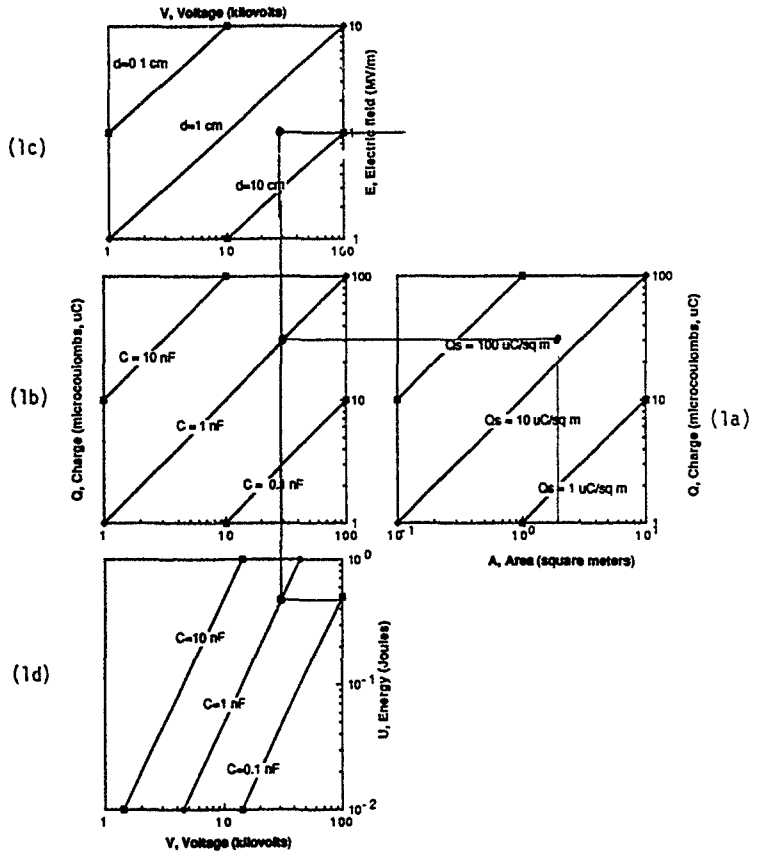

Figure 4.1 System Level Relationships Between Available Charge, Voltage, Field and Energy (See text for defining relationships and explanation of example)

All equations here were linear except the quadratic dependence of the available energy, U_a, on voltage, as seen in the steeper slope for Figure 4.1d. Figure 4.1 can be used to establish upper limits for the various quantities that may later be dictating an arc and possible ignition.

4.3 Microstructural Electro Magnetic Principles

We now look more closely at the possible values for discharge energy, to assure ourselves that they are not in fact greater than the available energy. Figure 4.2 shows four interconnected nomograms Although each nomogram can be used to find any variable as a function of the other two, we underline below the most likely variable to be solved for The four nomograms respectively are:

a. Lower left: Resistance vs voltage with current as a parameter

b. Upper left: Power vs voltage with current as a parameter

c. Lower right: Resistance vs Time with capacitance as a parameter

d. Upper right: Power vs time with power density as a parameter

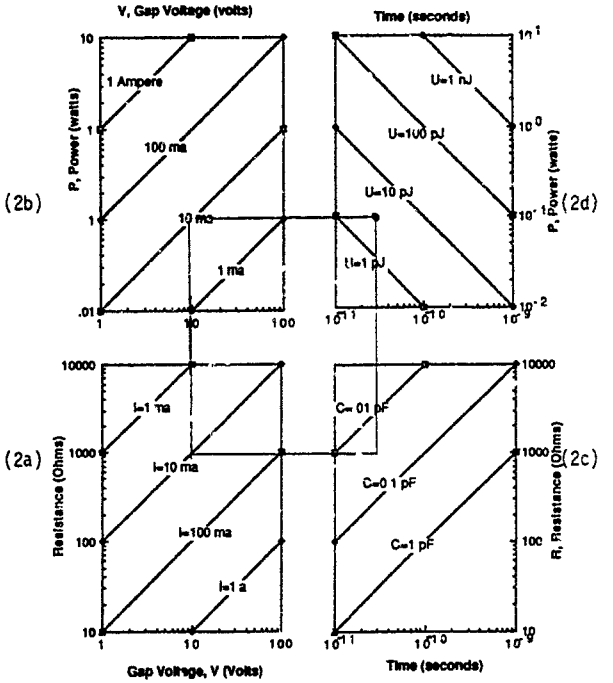

Figure 4.2 Discharge Parameters (Volts, Current, Resistance, Power, Capacitance, Time, Energy)

The equations for these nomograms are:

$$I = V / R \tag{4.2a}$$

$$P = I V \tag{4.2b}$$

$$t = R C \tag{4.2c}$$

$$U = P t \tag{4.2d}$$

By entering a voltage in Figure 4.2a (which can be obtained from later graphs, with knowledge of breakdown field and separation), and an assumed resistance (obtained from independent studies of breakdown physics), we can determine the likely current between the discharging spheres, using Eq. 4.2a. In the example shown, we assume 10 volts and 1000 amperes, giving a current of 10 milliamperes (ma). In fact, we know that both the voltage and the resistance are time-varying, so the current certainly is also. The graph should only be used to get an average value.

Traveling upward with the same voltage to Figure 4.2b, and using the currents just obtained (alternatively, we could have used the resistance with the formula $P = V^2/R$), we can obtain the power (time rate of change of energy deposited), using Eq. 4.2b. A possible error can creep in here, since the currents are reversed from their order in Figure 4.2a. In the example, we obtain a power level of 0.1 Watts.

In the lower right quadrant, we have a means of determining the time scale of the discharge, using Eq 4.2c The time, t, is read off of the abscissa, with the discharge resistance, R entered on the ordinate, using an assumed intersphere capacitance, C. In the example, we take C= 0.03 picofarads, so the assumed R of 1000 ohms gives a discharge time of 3 E-11, or 30 picoseconds.

In the upper right quadrant, the results obtained from Figure 4.2b and 4.2c are combined to allow an independent determination of the energy deposited by the arc, using Eq. 4.2d. In the example, we find about 3 picojoules. The energy so obtained should not be larger than the available energy obtained from the charge transfer

$$U_d = \int I V \, dt = V \int I \, dt = 0.5 \, Q \, V = 0.5 \, C \, V^2 \tag{4.2e}$$

To this point, we have established a system level vulnerability energy and a discharge level susceptibility energy (this section). Although a breakdown is assumed to have occurred, it is not obvious that an ignition will

ensue. This is the subject of the next section, where we first concentrate on those physical changes (other than ignition) that will first result from the breakdown

4.4 Ignition

Our available experimental information on the power or energy density required for ignition comes from laser and ESD experiments A major difference in the form of energy application is that the vast majority of the laser energy can be applied right at the surface which must be heated up to attain an ignition Only reflection of the laser beam causes inefficiency; this is sometimes controlled through darkening additives Electric sparks, on the other hand, typically demand a large voltage drop within the propellant or along its surface, which is only peripherally useful in heating the surface. This large energy may possibly be minimized by using low resistances, but this in turn leads to shorter arcs and a higher power density (but not energy density) requirement. Current breakdown experimental research will eventually lead to a good understanding of this trade-off with different resistances. In an operational (not laboratory) situation, there is a selection process which will lead to those being the most sensitive naturally occurring first.

Another difference is that the arc diameter can be much less than the several millimeters used in laser experiments. For small currents and higher pressures, diameters are estimated to be no more than a few microns (hence appreciably less than a millimeter). However, with an arc to a surface, the arc also is known to move around, so we might first start with a 1 square millimeter as a possible area. In laboratory simulations, the length of the arc may only be about 1 mm, so the area of the majority of the energy deposition may be even less than 1 sq mm

One other large difference for electric spark-caused ignition is that the entire arc is at high temperature -- not only the surface. As the binder and ammonium perchlorate decomposes, the reaction products will be ionized and (it is believed) can thereby more readily react in or near the arc. Since these reactions are exothermic (they release energy), it seems possible that the electric arc may be more efficient than the lasers in causing ignition Future research will possibly confirm this, when the full energy balance is understood.

Breakdown conditions are sometimes cited as being equivalent to ignition in terms of defining a serious safety hazard. Indeed, serious concerns have been raised by the observation that ignition seems to have been well underway (before stopped by propellant cracking) without a full discharge across test samples [Ref. 28] There is little experimental data on the amount of energy that is associated with these anomalous conditions, but the required external energy would appear to be on the order of picojoules However, experimental testing also shows that there are substantial differences - certainly in most experiments, few breakdowns do lead to ignition. However, we should note that in high pressure test configurations, other investigators do find that most discharges will lead to ignition.

4.5 Micro-Discharge Damage

Here, we explore obtaining a hazardous situation with micro-discharges (tiny arcs that occur between small spheres) of very small energy content. Although the energy content is low, the power density can be very high, given the small dimensions of an arc between spheres. We will explore this question with the set of nomograms in Figure 4.3. The primary quantities of interest are the breakdown field and discharge energy. The required equations are:

$$E = V/h \tag{4.3a}$$

$$U = .5\, C\, V^2 \tag{4.3b}$$

$$U = C_v\, dT\, v_c \tag{4.3c}$$

$$v_c = p\, r^2\, h \tag{4.3d}$$

$$A = 2\, p\, r\, h \tag{4.3e}$$

$$U_d = U / A \tag{4.3f}$$

where,

E	=	electric field
V	=	voltage
h	=	height of discharge
U	=	discharge energy
U_d	=	discharge energy density
C	=	capacitance
C_v	=	constant volume specific heat
dT	=	temperature change
v_c	=	arc cylinder volume.
A	=	arc cylinder lateral area

Each equation is plotted in the six parts of Figure 4.3. Our principal interest is in determining the radius of the arc, assuming that the breakdown occurs. Solving the set of equations 4.3, we find:

$$r = E\,(C\,h)^{-5} / (6.28\,C_v dT)^{5} \qquad (4.3g)$$

However, the effects of the four separate parameters (E,C, h, C_vdT) are hard to visualize, and the nomogram gives a more compact visualization of the relationships. Figure 4.3a (lower left diagram) allows us to specify an assumed cylinder height and breakdown field. In our first example, we assume that an average field of about 10 MV/m might be sufficient (this is possibly low), giving a sphere to sphere voltage of about 50 volts. This is an appreciably larger voltage than required for breakdown across say 100 microns of aluminum oxide with a breakdown field strength of perhaps 1 GV/m, where only about 10 volts would be required.

Traveling upwards to Figure 4 3b, we can intersect with capacitive lines near 0.01 picofarads, appropriate to a 20 micron sphere size (using C=4πεa for a single sphere). Even with the closer spacing of the 100 angstrom example of case 2 (and consequent higher capacitance), we deduce that the case 1 energy is higher by almost a factor of 10, with an energy of 12.5 picojoules.

We assume a thermal capacity of 10^6 joules per cubic meter per degree Kelvin and a desired temperature rise of 1000 degrees, so the C_vdT product is 10^4. This value of thermal capacity needs more research (that is currently under way), but the use of nomograms allows a rapid determination of the sensitivity of this parameter. To keep the units manageable, we convert to picojoules and cubic microns (with a cubic micron denoted as cu in the figure and 1 cu=10^{-18} cubic meters, making the appropriate diagonal labeled 1000 pj/cu). We thus predict approximately .012 and .0015 cubic microns (cu) respectively for the two cases.

Traveling downwards to part d of Figure 4.3 to find a cylinder radius (using Eq. 4.3d), we find about 0.03 and 0.5 microns respectively. The aspect ratios (h/r) for the two cases are very different - about 167 and 0.02, the former a long thin cylinder and the latter a disk-shaped object. The temperatures predicted here would not be achieved, since we are violating the assumption of a relatively homogeneous material, with the large aluminum spheres so nearby in case 2.

Part e of this figure (lower right) carries the computation of the radius (obtained in part d) an additional step to obtain the lateral surface area of the cylindrical discharge path, using Eq. 4.2e. The lower part of this figure is not valid for estimating energy transfer, since the height of the cylinder is there smaller than the radius. However, the nomogram still accurately gives the lateral surface area. With this qualification, the "total" area for dissipation of energy in the discharge is read along the abscissa of Figure 4.3e. Note the closer spacing of the r diagonal lines, since the lateral area is only dependent on the first power of the radius (Eq. 4.3e), whereas the volume of Figure 4.3d is dependent on the second power. In the example shown, a lateral area of 3 square microns (abbreviated su) is shown.

Traveling upward to Figure 4.3f, we can bring the energy obtained in Figure 4.3c over horizontally, and find at the intersection the energy density, using Eq. 4 3f. In this example the energy density is about 3 picojoules per square micron. This value of energy density can then be used to determine the likelihood of ignition using the ignition characteristics of the next section

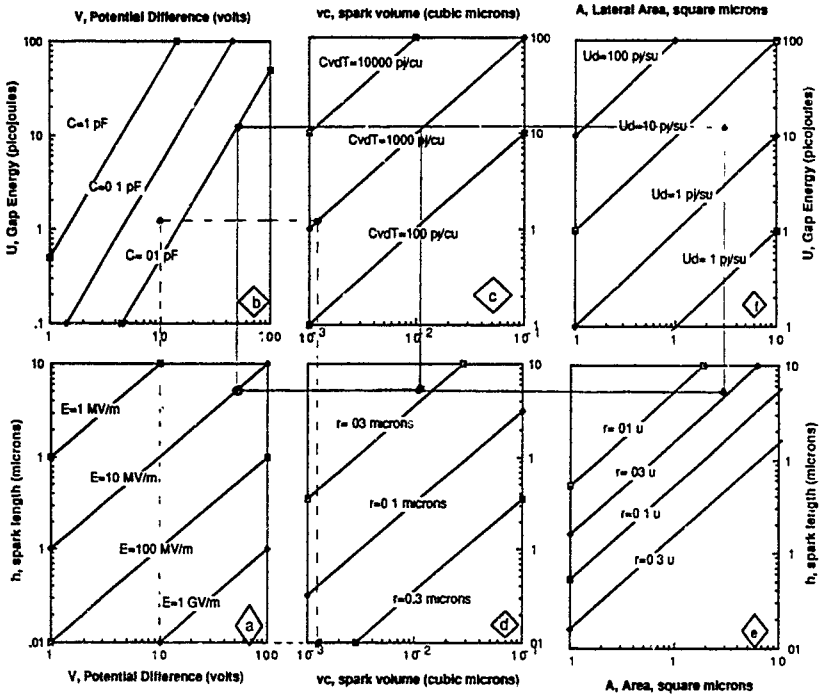

Figure 4.3 Characteristics of the Discharge Arc: Voltage, Field, Height, Capacitance, Volume, Radius, Area, Energy and Energy Density (Surface and Volume)

4.7 Ignition Characteristics

Figure 4 4 introduces the subject of ignition characteristics Here the interest is in the magnitude of the power and energy densities that are required to cause ignition as a function of the length of time of application of the power or energy The new aspect of this is the continuation of familiar arguments into the regime of sub

nanosecond pulses. Here the anchor value is taken as 1 watt per square mm at 100 milliseconds (based on data in Hermance [Ref. 2], showing approximately 25 calories per cm2-sec, and private communications with workers in the field [Ref. 15], giving about the same value). We see that at the lowest time scale on the graph (10^{-11} seconds), approximately 100 kW/sq mm is required for ignition - five orders of magnitude greater than for a time of 0.1 seconds. However, note that this power level seems more manageable when considered at a micron level - it is only 0.1 watts per square micron. Figure 4.4a also shows a cross-hatched region of departure from the -2 slope, due to insufficient pressure. In this region, an increase in pressure is required to return to the original slope

Figure 4.4b shows the same plot as it is displayed by individuals interested in ESD damage of electronic parts Now the slope is seen to have a value of -0.5. Although the electronics damage specialist also talks of a slope of negative .5, that person is talking only of melting, and of course not of ignition as we are doing here However, the similarity in slopes and presentation is of course because both are explained as thermal phenomena The change in slope due to pressure appears different in Figure 4 4b, but is of course due to the same phenomenon This phenomenon is not noted in the electronic parts literature, where they are normally looking at damage deep inside a high resistivity portion of a multi-layered chip, and the thermal melting is unaffected by external pressures

The presentation reversal of Figure 4.4b is especially useful in going to Figure 4 4c, which shows the energy in the same ignition event. Most importantly, the energy required for ignition actually decreases with decreasing time (or increases with increasing time). As the product of power and time, the log energy vs log time plot is found to gave a slope of -.5 + 1 = +.5 This is relatively easily perceived in Figure 4 4c, with a simple increase in the slope by the power of 1, due to the multiplication of power by time to obtain energy The reduction of the GO area due to insufficient pressure is now seen as a horizontal line defining a region in which reduction of time is no longer able to cause ignition, as it is above and to the right of that line

The main advantage of this presentation is seen in Figure 4.4d, which is the companion to Figure 4 4a, but with a slope of +2 This exponent is not immediately obvious, nor is the behavior with insufficient pressure The most important feature of the graph are the very low values of energy seen with short time depositions If one could get all the way to point 2 on this plot, then a deposition of only 1 microjoule per square mm in 10^{-11} seconds is predicted to be adequate Expressed in terms of picojoules and square microns, this is the same number- 1 picojoule per square micron.

These energy and temperature values seem reasonable in terms of what we know about the problem, although they are much smaller than experimentally reported values known to have caused an ignition The lowest ignition energy we know of is on the order of millijoules for a 1 inch sample Microjoules are reported for one case when extreme pressure was also present We think that a lot of the remaining difference can be made up as the energy contained in multiple breakdowns involving large strings of particles

The remaining variable to worry about is the energy and temperature increase required for the Ammonium Perchlorate particles to participate in a chemical reaction This will depend greatly on the size of the AP particle, which generally is much larger than the volume calculated above for the discharge volume This is presumably why sufficient energy is available to melt (perhaps vaporize) the alumina (and a small amount of aluminum), but not enough to cause ignition.

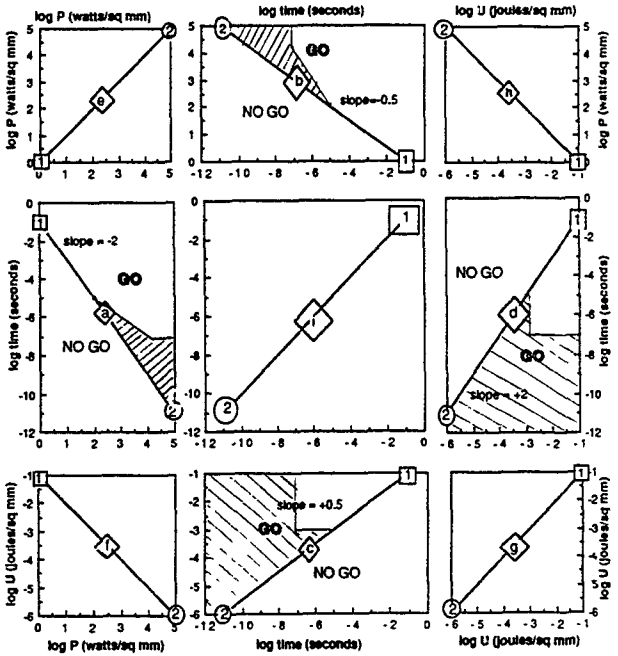

Figure 4.4 Hypothetical Propellant Ignition Characteristics

4.8 SUMMARY

This chapter has attempted to provide a brief introduction into present understanding about the ESD-caused ignition hazard with solid propellants. Although the understanding is still imperfect, much has been learned since the 1985 Pershing II accident. It is clear that the hazard can be primarily attributed to the close proximity of aluminum particles, which can preferentially cause a breakdown through a propellant rather than around it.

We have attempted to develop a graphical mechanism for demonstrating the inter-relationships between all of the many ESD variables - both for ESD and for ignition It is believed that these nomograms show all the various major trends more clearly than would tabulations or multiple graphs with parametric variations. The primary critical variables are the diameters and spacing of particles

Secondly, we have explored quantitatively the possibility that the amount of energy available in a micro-discharge might be sufficient to cause an ignition, using an extrapolation of experimental results obtained for longer times of power application. It seems likely that the energy is available to cause material melting and vaporization over a radius of about one thousand angstroms (0.1 micron), when the gap length is large. More work is required to determine the likelihood of the large spacings required to see the larger energies We do not believe that we have proved the possibility that internal micro-discharges are adequate to cause an ignition, but we do believe that we have shown it is possible.

Primary among the areas requiring more research are more accurate measures of the arc resistance More accurate determination of parameters such as the duration of the micro-discharges will enable the resistance to be determined. The analysis of the micro-discharge is found to be much more complicated than the corresponding macro-analysis. Significant additional research is required.

CHAPTER 5
SAFETY OVERVIEW

The previous material has summarized the final analytical work at EMA dealing with ESD breakdown This has primarily dealt with the "generic" microscopic analyses that we have performed under ARO sponsorship However, there is another large body of work, both at EMA and elsewhere that has dealt with specific motor configurations that could not be covered in this study and this report. Although much can be learned from the general, non-specific analyses, the specific analyses are necessary to ensure safety for specific systems.

Although the subject of safety was not a major part of our research, it has an overwhelming importance to the industry and individuals who will be interested in this report. Thus we feel it appropriate to close this report with a summary of what we know about safety issues identified through general truths, which are summarized in terms of the four main ESD areas described in Reference 2.

Charge Generation Safety

a. Materials should be selected which minimize the initial electrostatic generation Although this rule is often contradictory with other requirements (for minimum friction for example), the motor manufacturing community has been able to find replacement materials that are proving satisfactory.

b. Conductive materials are generally less likely to generate charge.

c. Proper grounding can rapidly remove charge.

Geometric Field Enhancement Safety

a. Design of solid propellant motors must take account of the ESD hazard in the future, but it is almost impossible to introduce a modification into an existing design Proper design will ensure adequate spacing of metal parts and will avoid sharp corners that can augment the interior fields.

b. Metal shielding can prevent large fields through the "Faraday" shielding phenomenon. This is especially important for lightning safety. Enclosing propellants in a metallic enclosure is the best means of ensuring safety The use of carbon fibers in composite cases is an excellent alternative

c. Applying conductive paint to nonmetallic enclosures is of high importance This approach has been used retroactively with several motor systems and has been under consideration with other fielded systems. Inspection programs should be in place to ensure that these paints are adequately connecting the metallic parts of the motor to the non-metallic

d. Grounds must be in place to tie all parts of the motor together. Personnel must understand the function of the grounding systems through training programs. In some circumstances, personnel should use personal wrist straps during handling operations.

Microscopic Field Enhancement Safety

a. The size of the aluminum and other particles are primarily dictated by specific energy requirements and considerations other than ESD. However, the wide range in breakdown fields among different propellant formulations suggests that a great deal of ESD safety improvement can be obtained if more attention is given to the formulation. The primary task will be to keep the aluminum particles separated. The use of smaller ammonium perchlorate particles is an important first step in this direction.

b The conductivity of the binder is especially important in establishing safety, with additives being helpful to increase conductivity.

Ignition Safety

a. Pressure and confinement are extremely important in going from a relatively insignificant breakdown to the more catastrophic ignition. Steps must be taken, especially during the manufacturing process, to ensure that friction is low and that mechanical pressures are minimized, whenever electric charges may be present.

b. Since discharge time is so important, with the shorter discharges being more hazardous, sufficient resistance must be in the grounding paths as to avoid a very rapid discharge Slow discharge (microseconds or milliseconds) is better than rapid (picosecond) discharge

References

1. Gyure, Mark F., "Theory of Dielectric Breakdown in Randomly Inhomogeneous Materials," EMA-90-R-50, December 1991.

2. Larson, R.W., et al ., "Microstructural Modeling of Electrical Breakdown in Solid Fuel Propellants," EMA-89-R-37, April 5, 1989.

3. Mann, D. M., et al., "Workshop Summary: ESD Ignition of Composite Solid Propellants," April 4, 1990, presented at the JANNAF Propulsion Systems Hazards Subcommittee Meeting.

4. Gyure, Mark F. and Paul D. Beale, "Dielectric Breakdown of a Random Array of Conducting Cylinders," Physical Review B 40, 9533 (1989).

5. Gyure, Mark F. and Paul D. Beale, "Modeling of Dielectric Breakdown in Metal-Loaded Dielectrics: Theory" presented at the Joint Army, Navy, NASA, Air Force (JANNAF) Propulsion Systems Hazards Subcommittee Meeting at the Johns Hopkins Applied Physics Laboratory in Laurel, Maryland, April 3-5, 1990.

6. Beale, Paul D. and Mark F. Gyure, "Modeling of Dielectric Breakdown in Metal-Loaded Dielectrics Applications" presented at the Joint Army, Navy, NASA, Air Force (JANNAF) Propulsion Systems Hazards Subcommittee Meeting at the Johns Hopkins Applied Physics Laboratory in Laurel, Maryland, April 3-5, 1990.

7. Hansen, J. P. and I.R. McDonald, Theory of Simple Liquids, (Academic, New York, 1976).

8. Perkus, K. and G.J. Yevick, Physical Review 110, 1 (1958).

9. Wertheim, M. S., Physical Review Letters 10, 321 (1963).

10. Theile, E., J. Chemical Physics 39, 474 (1963).

11. Lebowitz, J. L., Physical Review 133, A895 (1964)

12. Covino, J. and F. Hudson, "Current Assessment Methodology for Electrostatic Discharge Hazards of Energetic Materials," Journal of Propulsion and Power, 1990.

13. Larson, R. W., "An Overview of the Ignition of Solid Propellant by ESD and Transient Phenomena,' presented at the 1988 International Aerospace and Ground Conference on Lightning and Static Electricity, April 19-22, 1988, Oklahoma City

14. Larson, R. W., "Analytical Considerations in the ESD-Caused Ignition of Solid Propellants, presentation at JANNAF Conference, Laurel, MD, April 4, 1990 (Based on ARO work)

15. Hermance, C. E., "Solid Propellant Ignition Theories and Experiments," Chapter 5 in K K Kuo, Fundamentals of Solid Propellant Combustion, Vol 90, Progress in Astronautics and Aeronautics, 1984